

Majorana qubit readout by a point-contact detector under finite bias voltages

Huizi Xie,¹ Sirui Yu,¹ Hong Mao,^{1,*} and Jinshuang Jin^{1,†}

¹*School of Physics, Hangzhou Normal University, Hangzhou, Zhejiang 311121, China*

(Dated: June 18, 2024)

In this work we revisit the problem of four Majorana-zero-modes (4-MZMs) qubit readout by a point-contact (PC) detector. The logic states of the 4-MZMs qubit are converted to different charge occupations of a tunnel-coupled quantum dot (QD), which is further measured by a nearby PC detector. This type of measurement in principle requires that the PC detector is to be biased at small voltages, which should be comparable to the energy scales of the QD level and its coupling to the qubit. Going beyond existing studies on this problem, we present a unified treatment for both the steady-state current and the current power spectrum, which allow us to infer the qubit state information from either the QD occupation or the characteristic peak at the oscillation frequency. Moreover, we carry out the peak-to-pedestal ratio of each single characteristic peak (associated with each logic state of the qubit) and the signal-to-noise ratio of the two peaks. From these two figures of merit, we reveal the optimal bias voltage window for the PC detector at low temperature limit.

I. INTRODUCTION

Owing to the unique nature of non-Abelian statistics and spatial nonlocality, Majorana zero modes (MZMs) have a potential application in topological quantum computations [1–8]. Largely based on the MZMs which may be realized from the semiconductor/superconductor hybrid structures [9, 10], a variety of Majorana qubits have been proposed, such as the Majorana box qubits (MBQs) [7], tetrtons and hexons [8]. For the Majorana topological quantum computation, the qubit measurement is an important problem to be studied in the relatively early stage. Indeed, for instance, for the readout of MBQs, a variety of schemes have been proposed [7, 11–16], such as measuring the frequency shift of a double-dot system [7], dispersive shift from qubit-resonator interaction [12], and interferometric conductance [13, 14]. In particular, we are aware of the recent scheme of four-MZMs qubit readout by a point-contact (PC) detector [7, 8], where the fermion parity of the qubit is converted to occupation of a tunnel-coupled quantum dot (QD) [15, 16]. In Ref. 15, it was found that the scheme by means of measuring the steady-state QD occupation can be effective only under low bias voltage. On the contrary, in Ref. 16, instead of QD-occupation dependent current measurement under low bias voltage, a scheme based on measuring the power spectrum of the PC detector current was analyzed, at a large-bias-voltage limit.

In this work, we revisit the problem of 4-MZMs qubit readout analyzed in Refs.[15, 16]. Going beyond their existing studies, we present a unified treatment for both the steady-state current and the current power spectrum under finite (small) bias voltages, which allow us to infer the qubit state information from either the QD occupation or the characteristic frequencies in the current spectrum. We will carry out useful figures of merit, such as peak-to-pedestal ratio and signal-to-noise ratio, and reveal optimal bias voltage window for the PC detector at low temperature limit.

The paper is organized as follows. In Sec. II, we first give the model description and outline the basic measurement scenario. We then introduce the quantum master equation approach to calculate the transport current through the detector and the current power spectrum in a unified way. In Sec. III, we carry out the analytical and numerical results of the detector current. We also address the underlying physical mechanism of the parity-dependent current related to the bias voltage. In Sec. IV, the analytical and numerical results of the current power spectrum are illustrated. We further obtain the formula of the signal-to-noise ratio (*SNR*) of the two parity-dependent Rabi peaks. Especially, the optimal bias voltage window for the PC detector at low temperature limit is provided. Finally, we give our summary in Sec. V.

*Electronic address: mao@hznu.edu.cn

†Electronic address: jsjin@hznu.edu.cn

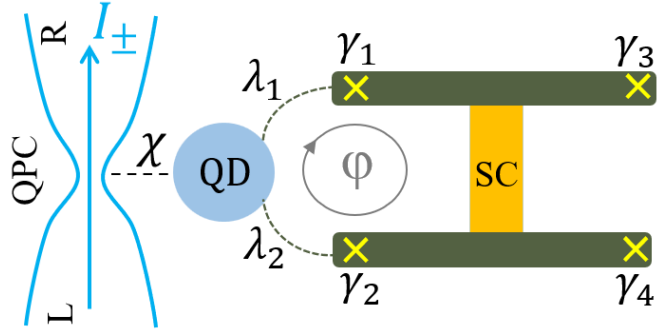


FIG. 1: (Color online) Schematic setup for the readout of a Majorana box qubit (MBQ). The MBQ is coupled to a quantum dot (QD) which is measured by a point-contact (PC) detector. The MBQ consists of two topological superconducting wires, hosting four Majorana zero energy modes $\gamma_1, \gamma_2, \gamma_3$ and γ_4 . The coupling of two Majoranas (γ_1, γ_2) and the QD leads to a parity-dependent current I_{\pm} through the PC detector.

II. METHODOLOGY

A. Model description

We consider a Majorana box qubit (MBQ) coupled to a quantum dot (QD), and the QD is in turn continuously measured by a voltage-biased point-contact (PC), as sketched in Fig. 1. The MBQ is formed in a floating superconducting island, consisting of two long topological superconducting nanowires [7, 8]. They each host a Majorana zero-energy mode (MZM) γ_i at both ends. Each pair of MZMs are related to the regular fermion through the transformation of $\gamma_1 = (\hat{f}_L + \hat{f}_L^\dagger)$, $\gamma_2 = -i(\hat{f}_L - \hat{f}_L^\dagger)$ for the left pair, and $\gamma_3 = (\hat{f}_R + \hat{f}_R^\dagger)$, $\gamma_4 = -i(\hat{f}_R - \hat{f}_R^\dagger)$ for the right pair, respectively. The corresponding occupation number operators are $\hat{n}_L = \hat{f}_L^\dagger \hat{f}_L$ and $\hat{n}_R = \hat{f}_R^\dagger \hat{f}_R$. Here, $\{\gamma_i, \gamma_j\} = 2\delta_{ij}$ and $\gamma_i^2 = 1$. The qubit states $|n_L n_R\rangle$ can then be encoded in the even parity space $\{|0_L 0_R\rangle, |1_L 1_R\rangle\}$ or odd parity space $\{|0_L 1_R\rangle, |1_L 0_R\rangle\}$.

The composite Hamiltonian of the device in Fig. 1 is $H_{\text{tot}} = H_{\text{S}} + H_{\text{B}} + H'$. The system is modeled by the low-energy Hamiltonian [15, 17],

$$H_{\text{S}} = \varepsilon_{\text{d}} \hat{d}^\dagger \hat{d} + \sum_{i=1,2} (\lambda_i \gamma_i \hat{d} + \text{H.c.}), \quad (1)$$

where we assume a pair of MZMs described by γ_1 and γ_2 and a single electronic level ε_{d} in the QD with the energy level of ε_{d} . The second term in Eq. (1) describes the tunnel coupling between the QD and two MZMs. Without loss of generality, the tunneling coefficients λ_i can be formally defined as, $\lambda_1 = |\lambda_1| e^{i\varphi_1}$ and $\lambda_2 = |\lambda_2| e^{i\varphi_2}$, and the gauge invariant phase difference $\varphi = \varphi_2 - \varphi_1$ can be tuned such as by varying the magnetic flux penetrating the enclosed area of the interference loop (see Fig. 1). The PC detector is described by the two electron reservoirs, $H_{\text{B}} = \sum_{\alpha k} \varepsilon_{\alpha k} \hat{c}_{\alpha k}^\dagger \hat{c}_{\alpha k}$ with $\alpha = L, R$. The interaction Hamiltonian between the dot and the PC detector is given by [18–20]

$$H' = \sum_{k,q} (\mathcal{T} + \chi n_{\text{d}}) \hat{c}_{Lk}^\dagger \hat{c}_{Rq} + \text{H.c.} \quad (2)$$

It describes the electron tunneling through PC, with the tunnel coupling amplitude that depends on electron occupation of the QD ($\hat{n}_{\text{d}} = \hat{d}^\dagger \hat{d}$). Here, we consider weak interaction with $\chi \ll \mathcal{T}$. For the later convenience, we introduce the system-related operator $\hat{Q} = \mathcal{T} + \chi \hat{n}_{\text{d}} = \hat{Q}^\dagger$ and the PC bath operator $\hat{F} = \sum_{kq} \hat{c}_{Lk}^\dagger \hat{c}_{Rq}$. The interaction Hamiltonian Eq. (2) is then straightforwardly rewritten as $H' = \hat{Q}(\hat{F} + \hat{F}^\dagger)$.

The measurement effects of PC reservoirs on the combined QD-MBQ system are characterized by the interaction bath correlation functions [21, 22], $C^{(+)}(t) \equiv \langle \hat{F}^\dagger(t) \hat{F}(0) \rangle_{\text{B}}$ and $C^{(-)}(t) \equiv \langle \hat{F}(t) \hat{F}^\dagger(0) \rangle_{\text{B}}$ with $\hat{F}(t) = e^{iH_{\text{B}}t} \hat{F} e^{-iH_{\text{B}}t} = \sum_{kq} \hat{c}_{Lk}^\dagger \hat{c}_{Rq} e^{i(\varepsilon_{Lk} - \varepsilon_{Rq})t}$. Here, $\langle \dots \rangle_{\text{B}}$ stands for the statistical average over the bath (PC electron reservoirs) in thermal equilibrium. The interaction bath spectrum is defined as the Fourier transform of the reservoir-electron correlation function [21, 23]

$$C^{(\pm)}(\omega) = \int_{-\infty}^{\infty} dt e^{i\omega t} C^{(\pm)}(t) = \frac{\eta x}{1 - e^{-\beta x}} \Big|_{x=\omega \mp V}, \quad (3)$$

which satisfies the detailed-balance relation $C^{(+)}(\omega) = e^{\beta(\omega-V)}C^{(-)}(-\omega)$ for arbitrary bias voltage $V = \mu_L - \mu_R$. Here we introduced the parameter $\eta = 2\pi g_L g_R$ under the consideration of the energy-independent density of states (g_L and g_R of the two reservoirs). Throughout this work, we adopt units of $e = \hbar = 1$ for the electron charge and the Planck constant.

B. Basic measurement scenario

Taking the even parity space ($\{|0_L 0_R\rangle, |1_L 1_R\rangle\}$) as a typical example, we give a brief description of the basic measurement protocol of the MBQ [15, 16]. During the entire measurement, the total parity of the superconducting island is assumed to be conserved. Therefore, the readout of the MBQ states $|0_L 0_R\rangle$ and $|1_L 1_R\rangle$ can map to the readout of the states $|0_L\rangle$ and $|1_L\rangle$, respectively. Then we can denote $|0_L\rangle$ ($\rightarrow |0_L 0_R\rangle$) and $|1_L\rangle$ ($\rightarrow |1_L 1_R\rangle$) as a logical qubit states. The readout of this logical qubit states can be realized by the measurement of the combined fermion parity of the dot and the left pair of MZMs (γ_1 and γ_2),

$$p = (-1)^{n_d + n_L}, \quad (4)$$

since this parity is conserved by the total composite Hamiltonian H_{tot} . For instance, the MBQ is assumed to be prepared in the initial state e.g., $|\psi_0\rangle = a|0_L\rangle + b|1_L\rangle$, with the complex coefficients a and b satisfying $|a|^2 + |b|^2 = 1$. The dot is supposed initially empty, $n_d = 0$. We then have the initial state of the dot-MBQ,

$$|\Psi_0\rangle = |0_d\rangle \otimes (a|0_L\rangle + b|1_L\rangle) = a|0_d 0_L\rangle + b|0_d 1_L\rangle. \quad (5)$$

Consequently, one knows that the MBQ state is $|0_L\rangle$ ($|1_L\rangle$) if $p = +1$ ($p = -1$) has been measured.

Described by the dot-MZM interaction Hamiltonian of Eq. (1), there are intrinsic coherent Rabi oscillations in the both subspaces of the odd parity $\{|0_d 1_L\rangle, |1_d 0_L\rangle\}$ ($p = -1$) and even parity $\{|0_d 0_L\rangle, |1_d 1_L\rangle\}$ ($p = +1$). The former is induced by the electron normal tunneling processes, and the latter arises from the Andreev reflection processes. That is, the Hamiltonian Eq. (1) can be written as,

$$H_s = \begin{pmatrix} H_- & 0 \\ 0 & H_+ \end{pmatrix}, \quad (6)$$

where the parity-dependent Hamiltonian in each subspace is

$$H_{p=\pm} = \begin{pmatrix} 0 & \lambda_1 - ip\lambda_2 \\ \lambda_1^* + ip\lambda_2^* & \varepsilon_d \end{pmatrix}. \quad (7)$$

Apparently, H_p indicates the intrinsic coherent Rabi oscillation. The corresponding Rabi frequency (Δ_p) reads,

$$\Delta_p = \sqrt{\varepsilon_d^2 + 4\lambda_p^2(\varphi)}, \quad (8)$$

with

$$\lambda_p^2(\varphi) \equiv |\lambda_1|^2 + |\lambda_2|^2 + 2p|\lambda_1||\lambda_2|\sin\varphi.$$

Note that the Rabi frequency Δ_p is the energy difference between the two eigenstates ($\{|e_p\rangle, |g_p\rangle\}$) of H_p , i.e., $\Delta_p = \varepsilon_{e_p} - \varepsilon_{g_p}$, with the excited energy $\varepsilon_{e_p} = (\varepsilon_d + \Delta_p)/2$ and the ground energy $\varepsilon_{g_p} = (\varepsilon_d - \Delta_p)/2$. The resulting Rabi frequency expressed by Eq. (8) is a periodic function of φ with 2π periodicity and parity dependent for $\varphi \neq k\pi$.

Thus, the MBQ can be in principle read out via any Δ_p -dependent observable quantities with $\varphi \neq k\pi$, such as the dot occupation number, the detector current, and the current power spectrum. It has been demonstrated in Ref. [15] that the readout of MBQ from the dot occupation number is effective only at low bias voltage. On the contrary, in Ref. [16], it has been analyzed that the information on the parity is not carried by the average current as well as the dot occupation number, but generically encoded in the power spectrum of the detector current at large bias voltage limit. In the present work, we will revisit such measurement problem at any bias voltage regime. We will explore the underlying physical mechanism and reveal the optimal bias voltage window for the PC detector for the readout of MBQ in the current power spectrum. All studies on the steady-state dot occupation number, detector current and its power spectrum will be uniformly based on the quantum master equation approach as introduced below.

C. Quantum master equation approach

It is well-known that the primary QD-MBQ system is described by the reduced density operator $\rho(t) \equiv \text{tr}_B[\rho_{\text{tot}}(t)]$, i.e., the partial trace of the total density operator ρ_{tot} over the bath space (the electron reservoirs of PC detector). Regarding the interaction Hamiltonian H' in Eq. (2) as a perturbation and adopting the Born-Markovian approximation, one can easily get the master equation for QD-MBQ system. It reads [23–25],

$$\dot{\rho}(t) = -i\mathcal{L}\rho(t) - \mathcal{R}\rho(t), \quad (9)$$

where the first term, $\mathcal{L}\bullet \equiv [H_s, \bullet]$, describes the coherent dynamics and the second term,

$$\mathcal{R}\bullet \equiv \frac{1}{2} [Q, \mathcal{Q}\bullet - \bullet\mathcal{Q}^\dagger], \quad (10)$$

arises from the measurement back-action of the PC detector. The resolvent operators are $Q = \mathcal{T} + \chi n_d$ and $\mathcal{Q} = \mathcal{Q}^{(-)} + \mathcal{Q}^{(+)}$, with $\mathcal{Q}^{(\pm)} \equiv C^{(\pm)}(-\mathcal{L})Q$. Here, the bath correlation function $C^{(\pm)}(-\mathcal{L})$ is given by Eq. (3) and satisfies the detailed-balance relation for arbitrary bias voltage. The Liouvillian operator “ \mathcal{L} ” in the correlation function $C^{(\pm)}(-\mathcal{L})$ contains the information of energy transfer between the detector and the measured system. In the eigenstate basis $\{|e_p\rangle, |g_p\rangle\}$, “ \mathcal{L} ” would be replaced by “ Δ_p ” which enters the correlation function, i.e., $C^{(\pm)}(\pm\Delta_p)$. All the observable quantities measured by PC detector as demonstrated below are closely related to $C^{(\pm)}(\pm\Delta_p)$, thus they carry the information of the parity.

For the calculation of the current through PC detector and its power spectrum, one can extend the master equation of Eq. (9) into the number-resolved (conditional) master equation and/or its conjugate counting field formalism [26, 27]. An alternative method is the introduction of the current-related density operator based on the energy-dispersed dissipation decomposition [28]. In the framework of the Born-Markov approximation, we can obtain the same formulas of the detector current and its power spectrum based on the above two methods as follows. Explicitly, the average current through PC detector is given by [22, 28]

$$I(t) = \text{tr}[\mathcal{J}^{(-)}\rho(t)], \quad (11)$$

and its power spectrum can be calculated via

$$S(\omega) = 2\text{tr}[\mathcal{J}^{(+)}\bar{\rho}] + 4\text{tr}[\mathcal{J}^{(-)}\Pi(\omega)\mathcal{J}^{(-)}\bar{\rho}]. \quad (12)$$

Here the superoperators are defined as

$$\mathcal{J}^{(\pm)}\bullet \equiv \frac{1}{2} [\mathcal{Q}^{(-)} \pm \mathcal{Q}^{(+)}] \bullet Q + \text{H.c.}, \quad (13a)$$

$$\Pi(\omega) \equiv \frac{1}{i(\mathcal{L} - \omega) + \mathcal{R}}, \quad (13b)$$

and the stationary state $\bar{\rho} \equiv \rho(t \rightarrow \infty)$ is obtained by setting $\dot{\rho}(t) = 0$ in Eq. (9).

We would like to note that in the following numerical calculations, all energies are measured in (arbitrary) unit of λ . We set $|\lambda_1| = \lambda$ and $|\lambda_2| = 0.8\lambda$ for the consideration of a certain degree of the coupling asymmetry between the QD and MZMs in experiments. Moreover, we consider weak interaction between the PC detector and the QD with $\mathcal{T} = \lambda$ and $\chi = 0.2\lambda$ in Eq. (2). The energy-independent density of states with $g_L = g_R = \lambda$ and finite temperature $k_B T = 0.5\lambda$ are adopted throughout the paper, unless otherwise stated. .

III. THE STEADY-STATE CURRENT

By replacing $\rho(t)$ with $\bar{\rho}$ in the expression of Eq. (11), the steady-state current is obtained as

$$\begin{aligned} I_p &= g_u V - \frac{1}{2}(g_u - g_v)V \left[1 + \frac{\Delta_p}{G^{(+)}(\Delta_p)} \right] \\ &\quad + g_b V \left[1 - \frac{\Delta_p}{V} \frac{G^{(-)}(\Delta_p)}{G^{(+)}(\Delta_p)} \right], \end{aligned} \quad (14)$$

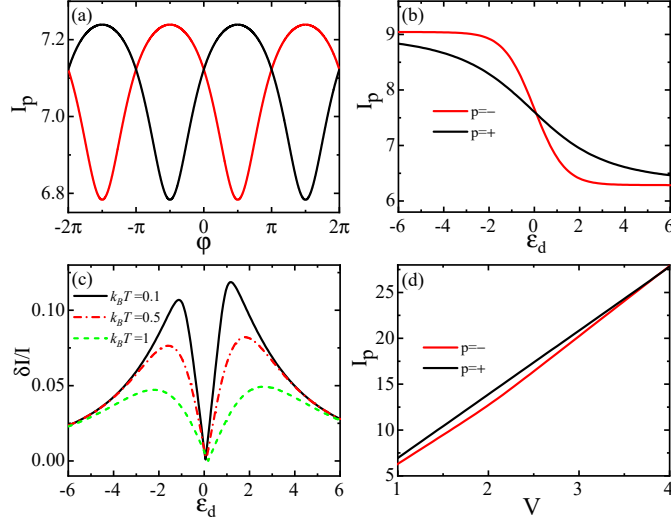


FIG. 2: (Color online) The parity-dependent steady-state current I_p (in $e\lambda/\hbar$) at low bias voltage $V = \lambda$, (a) as a function of flux φ with $\varepsilon_d = \lambda$ and (b) as a function of ε_d with $\varphi = \pi/2$. (c) The signal-to-current ratio as a function of ε_d with different temperature (in λ) for $\varphi = \pi/2$ and $V = \lambda$. (d) The detector current I_p as a function of the bias voltage for $\varphi = \pi/2$ and $\varepsilon_d = 2\lambda$.

where, $g_u = \eta u^2$, $g_v = \eta v^2$, and $g_b = \eta |b|^2$, with $u = \mathcal{T} + \frac{\chi}{2}(1 + \frac{\varepsilon_d}{\Delta_p})$, $v = \mathcal{T} + \frac{\chi}{2}(1 - \frac{\varepsilon_d}{\Delta_p})$, and $|b|^2 = \frac{\chi^2 \lambda_p^2(\varphi)}{\Delta_p^2}$. Here, we introduced

$$G^{(+)}(\Delta_p) \equiv \frac{C(\Delta_p) + C(-\Delta_p)}{2\eta}, \quad (15a)$$

$$G^{(-)}(\Delta_p) \equiv \frac{\bar{C}(\Delta_p) - \bar{C}(-\Delta_p)}{2\eta}, \quad (15b)$$

with $C(\omega) \equiv C^{(-)}(\omega) + C^{(+)}(\omega)$ and $\bar{C}(\omega) \equiv C^{(-)}(\omega) - C^{(+)}(\omega)$. Apparently, the steady-state current I_p in Eq. (14) is Δ_p -dependent through the bath correlation function $C^{(\pm)}(\pm\Delta_p)$ and its periodic variation with the flux is numerically shown in Fig. 2 (a). The MBQ can thus be read out from I_p for $\varphi \neq k\pi$. Especially, the signal $\delta I = |I_+ - I_-|$ is maximum at $\varphi = (2k + 1)\frac{\pi}{2}$ with k the integer.

Actually, the parity-dependent average current (I_p) is quite similar to that of the steady-state dot occupation number (n_p). Via the definition of $n_p = \langle \hat{d}^\dagger \hat{d} \rangle_p$, one can straightforwardly recover the result of $n_p = \frac{1}{2} [1 - \frac{\varepsilon_d}{G^{(+)}(\Delta_p)}]$ in Ref. 15. The dot occupation number n_p is parity-dependent via also the bath correlation function of $G^{(+)}(\Delta_p)$ (expressed by Eq. (15a)), and thus can read out the MBQ. Apparently, for $\varepsilon_d = 0$, the dot occupation number is simplified to $n_p = \frac{1}{2}$ and the steady-state current is also parity-independent as displayed in Fig. 2 (b). The reason is that the coherent dynamics between the two states in each subspace, e.g., $|00\rangle$ ($|01\rangle$) and $|11\rangle$ ($|10\rangle$) for even (odd) parity, are the equivalent Rabi resonances for $\varepsilon_d = 0$. Furthermore, we plot the signal-to-current ratio, i.e., $\delta I/I = |I_+ - I_-|/I$ with $I = \frac{I_+ + I_-}{2}$, as shown in Fig. 2 (c). It indicates that the read out of MBQ from the detector current I_p should away from (but nearby) the resonance of $\varepsilon_d = 0$ at low temperature regime with $k_B T \ll \lambda$.

Figure 2 (d) displays the steady-state current as a function of the bias voltage. Evidently, *in the large bias voltage regime*, i.e., $V \gg \Delta_p$, the current is parity-independent and thus cannot read out the MBQ. The behind reason can be understood as follows. In line with the expression of the current in Eq. (14), the involved correlation functions are simplified to be energy-independent, i.e., $C^{(+)}(\pm\Delta_p) = 0$ and $C^{(-)}(\pm\Delta_p) = \eta(V \pm \Delta_p) \rightarrow \eta V$ as can be inferred from Eq. (3) under large bias voltage limit. Physically, this is because the energy emitted/absorbed by the system (Δ_p) is negligible in comparison with the large bias voltage. That is, the average current in Eq. (14) becomes

$$I_p \rightarrow I_c = g_0 V + g_1 V, \quad (16)$$

where $g_0 = \eta(\mathcal{T} + \chi/2)^2$ and $g_1 = \eta(\chi/2)^2$. Apparently, the current in Eq. (16) under large bias voltage limit is independent of the parity. In fact, it can be easily obtained as $I_c = (I_1 + I_0)/2$ with $I_1 = \eta(\mathcal{T} + \chi)^2 V$ and $I_0 = \eta \mathcal{T}^2 V$, which are the currents corresponding to the dot states $|1\rangle$ and $|0\rangle$, respectively. Consequently, we cannot read out the

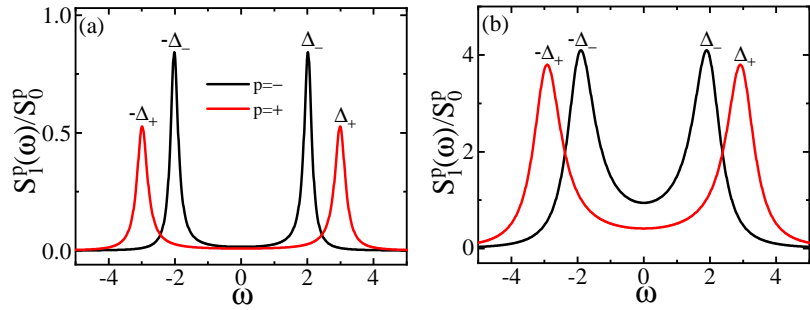


FIG. 3: (Color online) The finite-frequency current power spectrum for $\varepsilon_d = 0$ and $\varphi = \pi/8$ with (a) at low bias voltage $V = \lambda$ and (b) at large bias voltage $V = 8\lambda$.

MBQ from the detector current as well as the steady-state dot occupation number ($n_p \rightarrow 1/2$) at large bias voltage regime. Similar result has also been reported in Refs [15, 16].

Therefore, as far as the steady-state current and the dot occupation number are concerned, there have two conditions what should be satisfied for the readout of the parity number experimentally. One is that the energy level of the dot should be tuned away from the resonance ($\varepsilon_d \neq 0$). The other is that the applied bias voltage should be low with $V \lesssim \Delta_p$.

IV. POWER SPECTRUM

As well-known, the current power spectrum carries the information of the system beyond the average current. As we can infer from the formula Eq. (12), the power spectrum characterizes not only the back action of the detector described by the first term, but also the intrinsic coherent dynamics of the measured system depicted by the second term. This leads to that the current power spectrum is directly related to the parity-dependent Rabi frequency Δ_p and is not limited by both the dot energy level and bias voltage. Namely, as long as $\delta\Delta \equiv |\Delta_+ - \Delta_-| \neq 0$ with $\varphi \neq k\pi$, the MBQ can be read out from the current power spectrum as we will demonstrated in detail below. Consequently, for clarity, we will consider the resonance case with $\varepsilon_d = 0$ to get the analytical result of power spectrum, and take $\varphi = \pi/8$ as a typical example in the following numerical calculations.

Let us derive the analytical result of the current power spectrum based on the formula Eq. (12). For convenience, we separate the power spectrum into a frequency-independent part S_0^P and a frequency-dependent part $S_1^P(\omega)$, i.e., $S_p(\omega) = S_0^P + S_1^P(\omega)$. Explicitly, we get

$$S_0^P = 2g_0V \coth \frac{V}{2T} + 2g_1 \left[G_p^{(+)} - \frac{\Delta_p^2}{G_p^{(+)}} \right], \quad (17a)$$

$$S_1^P(\omega) = \frac{F_1(\Delta_p)\Gamma_p\Delta_p^2}{(\omega^2 - \Delta_p^2)^2 + \Gamma_p^2\omega^2} + \frac{F_2(\Delta_p)G_p^{(-)}}{\omega^2 + \Gamma_p^2}, \quad (17b)$$

where $G_p^{(\pm)} \equiv G^{(\pm)}(\Delta_p)$, $F_1(\Delta_p) = I_d^2 \left[1 - \frac{\Delta_p}{2V} \frac{G_p^{(-)}}{G_p^{(+)}} \right]$ with $I_d = I_1 - I_0$, $F_2(\Delta_p) = 8g_1^3 \left[2\Delta_p V - \Delta_p^2 \frac{G_p^{(-)}}{G_p^{(+)}} - G_p^{(-)} G_p^{(+)} \right]$. In particular, Γ_p in Eq. (17b) is the dephasing rate and it can be expressed as,

$$\Gamma_p = 2g_1 G_p^{(+)}(\Delta_p). \quad (18)$$

Furthermore, by taking the large bias voltage limit ($V \gg \Delta_p$), the power spectrum in Eq. (17) becomes

$$S_0^P \rightarrow 2I_p, \quad (19a)$$

$$S_1^P(\omega) \rightarrow \frac{I_d^2 \Gamma_d \Delta_p^2}{(\omega^2 - \Delta_p^2)^2 + \Gamma_d^2 \omega^2} + \frac{4g_1 \Gamma_d \Delta_p^2}{\omega^2 + \Gamma_d^2}, \quad (19b)$$

where the dephasing rate of Eq. (18) is simplified to $\Gamma_d = 2g_1 V = \eta V \chi^2 / 2$.

As we expected, the current power spectrum has more advantages over the steady-state current and the dot occupation number. Since the power spectrum given by Eq. (17) depicts the parity-dependent even for the resonance

case ($\varepsilon_d = 0$) at any bias voltages, including large bias voltage regime [see Eq. (19b)]. The MBQ can be read out via the locations of the parity-dependent peaks around the parity-dependent Rabi frequencies, i.e., $\omega \simeq \pm\Delta_p$. The peaks which come from the intrinsic coherent Rabi oscillation of the QD-MBQ system is determined by $\Pi(\omega)$ in the second term of Eq. (12).

The corresponding numerical results are illustrated in Fig. 3 (a) at low voltage ($V = \lambda$) and Fig. 3 (b) at large voltage ($V = 8\lambda$), respectively. We find that the raise of the measurement voltage leads to two effects on the power spectrum. One is the increase in the height of the peaks and the other is the enhancement of the peak width. The former is beneficial for the measurement, while the latter is not. Therefore, it is necessary to find the optimal bias voltage range of the PC detector for the qubit measurement visibility.

To characterize the effect of the voltage on the peak width, we recast the frequency-dependent power spectrum formula Eq. (17b) into the Lorentz form. After some algorithm, we obtain

$$S_1^p(\omega) \simeq \frac{4f(\Delta_p)F_1(\Delta_p)\Delta_p^2}{\Gamma_p(4\Delta_p^2 - \Gamma_p^2)} \sum_{\pm} \frac{\sigma_p^2}{(\omega \pm \tilde{\Delta}_p)^2 + \sigma_p^2} + \frac{g(\Delta_p)F_1(\Delta_p)\Gamma_p}{\Delta_p^2} \frac{\sigma_{0p}^2}{\omega^2 + \sigma_{0p}^2} + \frac{F_2(\Delta_p)G_p^{(-)}}{\omega^2 + \Gamma_p^2}, \quad (20)$$

where

$$\tilde{\Delta}_p = \sqrt{\Delta_p^2 - \Gamma_p^2/2} \approx \Delta_p, \quad (21a)$$

$$\sigma_p = \frac{\tilde{\Delta}_p}{2} \left(\sqrt{1 + \Gamma_p/\tilde{\Delta}_p} - \sqrt{1 - \Gamma_p/\tilde{\Delta}_p} \right) \approx \frac{\Gamma_p}{2}, \quad (21b)$$

$$\sigma_{0p} = \sqrt{\tilde{\Delta}_p^2 + \sqrt{\Delta_p^4 + \tilde{\Delta}_p^4}} \approx \sqrt{1 + \sqrt{2}}\Delta_p. \quad (21c)$$

Here, Eqs. (21) come from the consideration of the weak interaction between the QD and the detector with $\Gamma_p \ll \Delta_p$. Since the functions of $g(\Delta_p)$ and $f(\Delta_p)$ are quite complicated and they are not explicitly shown.

For the measurement visibility analysis, we further define the signal by the position difference between the two peaks of the even and odd parities,

$$\mathcal{S} \equiv \tilde{\delta}\Delta = |\tilde{\Delta}_+ - \tilde{\Delta}_-| \approx \delta\Delta. \quad (22a)$$

While the noise is defined by the sum of the peak widths of the two parities,

$$\mathcal{N} \equiv \sigma_+ + \sigma_- \approx \frac{1}{2}(\Gamma_+ + \Gamma_-). \quad (22b)$$

Therefore, the so-called signal-to-noise ratio (SNR) of the two characteristic peaks can be calculated via

$$SNR = \frac{\mathcal{S}}{\mathcal{N}} \approx \frac{2\delta\Delta}{\Gamma_+ + \Gamma_-}. \quad (23)$$

It indicates that the SNR which is proportional to $\delta\Delta$ is determined by the intrinsic quantities involved in the system's Hamiltonian of Eq. (1), such as the coupling coefficients λ_i and the flux φ . Whereas, SNR is inversely proportional to the dephasing rates given by Eq. (18) due to the back-action of the PC detector on the QD-MZM system. Hence, SNR is affected by both the applied bias voltage and temperature of the detector.

Figure 4 depicts that the SNR is reduced by increasing the measurement voltage, and even less than 1 at large voltage limit. Furthermore, at low bias voltage regime, the SNR is enhanced with the reduction in temperature. We now focus on the low temperature limit with $k_B T \ll \lambda$. Then the SNR of Eq. (23) is simplified to

$$SNR = \frac{4\delta\Delta}{\eta\chi^2(\Delta_+ + \Delta_-)}, \quad \text{for } V < \Delta_p, \quad (24a)$$

$$SNR = \frac{2\delta\Delta}{\eta\chi^2 V}, \quad \text{for } V \geq \Delta_p. \quad (24b)$$

Seemingly, the measurement voltage should be low at $V < \Delta_p$, since the SNR determined by Eq. (24a) reaches a maximum saturation value which is independent of the bias voltage. This feature can also be seen in Fig. 4 at low temperature with $k_B T = 0.1\lambda$.

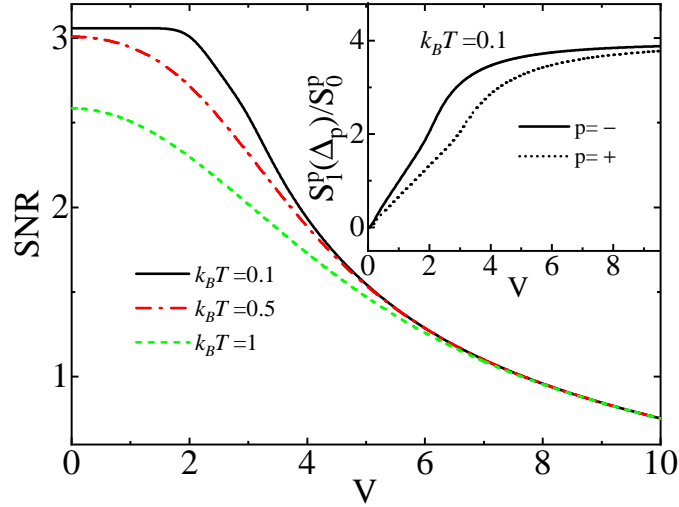


FIG. 4: (Color online) The *SNR* as a function of the bias voltage with different temperature (in λ). The inset is the peak-to-pedestal ratio as a function of the bias voltage at low temperature $k_B T = 0.1\lambda$. The other parameters are the same as in Fig. 3.

However, from the perspective of measurement visibility, we have to consider the height of the single peak in the experiments. That is, we have to consider another type of “signal-to-noise” ratio which is also known as *peak-to-pedestal* ratio of each single characteristic peak, i.e., $\gamma_p \equiv S_1^P(\Delta_p)/S_0^P(\Delta_p)$. In contrast with the *SNR* feature discussed above, the peak-to-pedestal increases with the bias voltage as shown in the inset of Fig. 4. It has the fundamental upper bound limit of 4 at high-voltage regime and also decreases with the increase in the temperature. This characteristic is consistent with the demonstrations in previous works [22, 29, 30].

Therefore, considering the merits of *SNR* and peak-to-pedestal ratio, the optimal condition of the measurement visibility should satisfy the relations of both $SNR > 1$ and $\gamma_p \rightarrow 4$ at low temperature limit. For $V < \Delta_p$, the *SNR* given by Eq. (24a) can easily satisfy $SNR > 1$, but $\gamma_p < 2$. So that the low bias voltage regime with $V < \Delta_p$ is not good for the MBQ measurement. For $V \geq \Delta_p$ in which $\gamma_p \lesssim 4$, the condition of $SNR > 1$ leads to $V < \frac{2\delta\Delta}{\eta\chi^2}$ as inferred by Eq. (24b). Consequently, we get the optimal range of the measurement voltage for the MBQ readout as,

$$\Delta_p \leq V < \frac{2\delta\Delta}{\eta\chi^2}. \quad (25)$$

Then, based on Eq. (25), all the parameters involved in the experimental measurement can be appropriately adopted. We believe it significantly simplifies the current experimental demonstrations.

V. SUMMARY

In summary, we have thoroughly investigated the detector current and its power spectrum at all voltages for the hybrid QD-MBQ system continuously measured by the PC detector. The analytical and numerical results have been carried out uniformly based on the Born-Markovian quantum master equation approach. It maintains the detail-balance relation and is potentially applicable for any bias voltage.

We have explored and demonstrated that the readout of the MBQ from the parity-dependent detector current as well as the dot occupation number is only suitable for low bias voltage situations. The underlying reason is that the parity information contained in the current (I_p) and the dot occupation number (n_p) is via the energy-dependent bath correlation function. It comes from the back-action of the detector and accounts for the energy exchange (characterized by the parity-dependent Rabi frequency Δ_p) between the measured system and detector. Nevertheless, the energy (Δ_p) emitted/absorbed by the QD-MBQ system is negligible in comparison with the large bias voltage. This leads to the energy-independent bath correlation function. Thus, I_p (also n_p) are parity-independent and cannot readout MBQ at large bias voltage regime ($V \gg \Delta_p$).

However, for the parity-dependent current power spectrum $S_p(\omega)$, the MBQ can be readout from the parity-dependent Rabi oscillation peak signals, in principle, at all bias voltage. This is because the current power spectrum

characterizes not only the back action of the detector described by the bath correlation, but also the intrinsic coherent dynamics of the measured system depicted by its intrinsic parity-dependent Hamiltonian. Importantly, for the measurement visibility analysis, we carry out the signal-to-noise ratio of the two parity-dependent characteristic peaks and the peak-to-pedestal ratio of each single peak. From these two figures of merit, we obtain the optimal bias voltage range of the PC detector for the MBQ readout at low temperature limit. The present results can enlighten the current experimental demonstrations.

Acknowledgments

We acknowledge helpful discussions with Prof. Xin-Qi Li and Prof. YiJing Yan. The support from the Natural Science Foundation of China (Grant No. 12175052) is acknowledged.

-
- [1] A. Y. Kitaev, “Unpaired Majorana fermions in quantum wires,” *Physics-Uspekhi* **44**, 131 (2001).
- [2] A. Kitaev, “Fault-tolerant quantum computation by anyons,” *Annals of Physics* **303**, 2 (2003).
- [3] C. Nayak, S. H. Simon, A. Stern, M. Freedman, and S. Das Sarma, “Non-Abelian anyons and topological quantum computation,” *Rev. Mod. Phys.* **80**, 1083 (2008).
- [4] M. Leijnse and K. Flensberg, “Quantum Information Transfer between Topological and Spin Qubit Systems,” *Phys. Rev. Lett.* **107**, 210502 (2011).
- [5] S. D. Sarma, M. Freedman, and C. Nayak, “Majorana zero modes and topological quantum computation,” *npj Quantum Inf* **1**, 15001 (2015).
- [6] D. Aasen, M. Hell, R. V. Mishmash, A. Higginbotham, J. Danon, M. Leijnse, T. S. Jespersen, J. A. Folk, C. M. Marcus, K. Flensberg, and J. Alicea, “Milestones Toward Majorana-Based Quantum Computing,” *Phys. Rev. X* **6**, 031016 (2016).
- [7] S. Plugge, A. Rasmussen, R. Egger, and K. Flensberg, “Majorana box qubits,” *New Journal of Physics* **19**, 012001 (2017).
- [8] T. Karzig, C. Knapp, R. M. Lutchyn, P. Bonderson, M. B. Hastings, C. Nayak, J. Alicea, K. Flensberg, S. Plugge, Y. Oreg, C. M. Marcus, and M. H. Freedman, “Scalable designs for quasiparticle-poisoning-protected topological quantum computation with Majorana zero modes,” *Phys. Rev. B* **95**, 235305 (2017).
- [9] R. M. Lutchyn, J. D. Sau, and S. Das Sarma, “Majorana Fermions and a Topological Phase Transition in Semiconductor-Superconductor Heterostructures,” *Phys. Rev. Lett.* **105**, 077001 (2010).
- [10] Y. Oreg, G. Refael, and F. von Oppen, “Helical Liquids and Majorana Bound States in Quantum Wires,” *Phys. Rev. Lett.* **105**, 177002 (2010).
- [11] A. L. Grimsmo and T. B. Smith, “Majorana qubit readout using longitudinal qubit-resonator interaction,” *Phys. Rev. B* **99**, 235420 (2019).
- [12] T. B. Smith, M. C. Cassidy, D. J. Reilly, S. D. Bartlett, and A. L. Grimsmo, “Dispersive Readout of Majorana Qubits,” *PRX Quantum* **1**, 020313 (2020).
- [13] L. Qin, X.-Q. Li, A. Shnirman, and G. Schön, “Transport signatures of a Majorana qubit and read-out-induced dephasing,” *New Journal of Physics* **21**, 043027 (2019).
- [14] K. Zhou, C. Zhang, L. Qin, and X.-Q. Li, “Double-dot interferometer for quantum measurement of Majorana qubits and stabilizers*,” *Chinese Physics B* **30**, 010301 (2021).
- [15] M. I. K. Munk, J. Schulenborg, R. Egger, and K. Flensberg, “Parity-to-charge conversion in Majorana qubit readout,” *Phys. Rev. Res.* **2**, 033254 (2020).
- [16] J. F. Steiner and F. von Oppen, “Readout of Majorana qubits,” *Phys. Rev. Res.* **2**, 033255 (2020).
- [17] K. Flensberg, “Non-Abelian Operations on Majorana Fermions via Single-Charge Control,” *Phys. Rev. Lett.* **106**, 090503 (2011).
- [18] S. A. Gurvitz, “Measurements with a noninvasive detector and dephasing mechanism,” *Phys. Rev. B* **56**, 15215 (1997).
- [19] A. N. Korotkov, “Continuous quantum measurement of a double dot,” *Phys. Rev. B* **60**, 5737 (1999).
- [20] H. S. Goan and G. J. Milburn, “Dynamics of a mesoscopic charge quantum bit under continuous quantum measurement,” *Phys. Rev. B* **64**, 235307 (2001).
- [21] X. Q. Li, W. K. Zhang, P. Cui, J. S. Shao, Z. S. Ma, and Y. J. Yan, “Quantum measurement of solid-state qubit: A unified quantum master equation approach,” *Phys. Rev. B* **69**, 085315 (2004).
- [22] X. Q. Li, P. Cui, and Y. J. Yan, “Spontaneous relaxation of a charge qubit under electrical measurement,” *Phys. Rev. Lett.* **94**, 066803 (2005).
- [23] R. X. Xu, Y. J. Yan, and X. Q. Li, “Cavity quantum electrodynamics in the presence of energy relaxation and pure dephasing: A unified quantum master-equation approach,” *Phys. Rev. A* **65**, 023807 (2002).
- [24] Y. J. Yan, “Quantum Fokker-Planck theory in a non-Gaussian-Markovian medium,” *Phys. Rev. A* **58**, 2721 (1998).
- [25] Y. J. Yan, F. Shuang, R. X. Xu, J. X. Cheng, X. Q. Li, C. Yang, and H. Y. Zhang, “Unified approach to the Bloch-Redfield theory and quantum Fokker-Planck equations,” *J. Chem. Phys.* **113**, 2068 (2000).
- [26] R. Zwanzig, *Nonequilibrium Statistical Mechanics*, Oxford University Press, New York, 2001.

- [27] Y. Makhlin, G. Schön, and A. Shnirman, “Quantum-state engineering with Josephson-junction devices,” *Rev. Mod. Phys.* **73**, 357 (2001).
- [28] Y. Xu, J. Jin, S. Wang, and Y. Yan, “Memory-effect-preserving quantum master equation approach to noise spectrum of transport current,” *Phys. Rev. E* **106**, 064130 (2022).
- [29] A. N. Korotkov, “Output spectrum of a detector measuring quantum oscillations,” *Phys. Rev. B* **63**, 085312 (2001).
- [30] R. Ruskov and A. N. Korotkov, “Spectrum of qubit oscillations from generalized Bloch equations,” *Phys. Rev. B* **67**, 075303 (2003).